

Phase Equilibria of the Mn-Si-Zn System at 600 °C

HONGHUI XU, XIANG XIONG, LIJUN ZHANG, YONG DU, and PEISHENG WANG

The phase equilibria at 600 °C of the Mn-Si-Zn system were investigated by using nineteen equilibrated alloys and two diffusion couples. The alloys were prepared by melting the pure elements in the alumina crucibles encapsulated in quartz tubes. The samples were examined by means of optical microscopy, X-ray diffraction, scanning electron microscopy (SEM), and electron probe microanalysis (EPMA). The experimental results showed no existence of ternary compounds in the Mn-Si-Zn system. The binary compound Mn_5Si_2 , the existence of which is controversial in the literature, were not observed at 600 °C. A massive phase transformation for (γ Mn) was observed due to its slow quenching. In addition, the controversial ε -phase region was studied. The existence of ε_1 was confirmed through a diffusion couple method. Though the existence of ε_2 (another controversial subdivision of the ε phase) was not confirmed, it is assumed to exist, taking into account the difference in the observed mechanical properties of the Mn-Zn binary alloys. The solubility of Zn in R- Mn_6Si , ν - Mn_9Si_2 , Mn_3Si , Mn_5Si_3 , MnSi, and $Mn_{11}Si_{19}$ was measured to be 1.3, 0.8, 0.5, 0.8, 0.5, and 0.2 at. pct Zn, respectively. The solubility of Si in (β Mn), (γ Mn), ε , and liquid was determined to be negligible.

DOI: 10.1007/s11661-009-9908-z

© The Minerals, Metals & Materials Society and ASM International 2009

I. INTRODUCTION

THINNER steel sheets for automotive applications imply higher demands in material strength and corrosion protection. Mn and Si are generally employed as the alloying elements for high-strength steels. The corrosion resistance of the steel sheets for the cars is significantly enhanced *via* galvanizing. Nevertheless, the behaviors of Si and Mn in the Si-Mn steels during galvanizing will influence the hot-dip galvanizability of the sheet steels.^[1] For the advanced development of the hot-dip galvanizing process for the high-strength steel sheets, knowledge of the phase equilibria in the Mn-Si-Zn system and information on the interaction between Mn, Si, and Zn are desirable.

The Si-Zn phase diagram without compound was thermodynamically evaluated by Jacobs and Spencer.^[2] The Mn-Si phase diagram was critically evaluated by Okamoto^[3] and thermodynamically assessed by Du *et al.*^[4] There is a general agreement on the existence of six intermediate compounds, *viz.* R- Mn_6Si , ν - Mn_9Si_2 , Mn_3Si , Mn_5Si_3 , MnSi, and $Mn_{11}Si_{19}$ (or $MnSi_{1.75-x}$). The existence and stability of the Mn_5Si_2 that was indicated as dashed lines in Reference 3 are still controversial. Okamoto and Tanner^[5] presented an assessed Mn-Zn phase diagram mainly based on the results of Wachtel and Tsiuplakis,^[6] Romer and Wachtel,^[7] and Nakagawa and Hori.^[8] There are several regions with uncertainties in the currently accepted Mn-Zn phase diagram.^[5] Controversy on whether the hexagonal

ε -phase has three different modifications (*viz.* ε , ε_1 , and ε_2) is still unresolved. Wachtel and Tsiuplakis^[6] performed magnetic susceptibility measurements on the zinc-rich Zn-Mn alloys. Their results indicated that the hexagonal ε phase can be subdivided into a region consisting of three phases, *viz.* ε , ε_1 , and ε_2 . However, the investigations by Romer and Wachtel^[7] and Nakagawa and Hori^[8] showed no indication of phase separation.

Up to now, no experimental information on the ternary Mn-Si-Zn system has been reported in the literature. So, the objective of this article is to perform an experimental investigation of the phase equilibria at 600 °C. The Zn-bearing alloys are prepared by melting the pure elements in the alumina crucibles encapsulated in quartz tubes because of the high evaporability of Zn.

II. EXPERIMENTAL PROCEDURES

Mn (99.9 wt pct), Si (99.999 wt pct), and Zn (99.99 wt pct) were used as starting materials. Prior to alloy preparation, Mn pieces were treated with nitric acid to remove the surface oxides; washed sequentially with water, ethanol, and acetone; and kept ready in acetone for use while Si and Zn had already been weighed. The accurately weighed ingredients (Mn pieces and blocks of Si and Zn) of nominal compositions given in Table I and shown in Figure 1 were put in small alumina crucibles that were then separately encapsulated in quartz tubes. The quartz capsules were put in an L4514-type diffusion furnace at 700 °C and then heated to temperatures between 850 °C and 1150 °C depending on the estimated liquidus temperatures of the alloys. After holding at the specific temperatures for 20 to 40 hours, the furnace was slowly cooled to 600 °C and the capsules were quenched in cold water. All the alloys prepared by the preceding process were annealed at 600 °C for 40 days in an

HONGHUI XU, XIANG XIONG, and YONG DU, Professors, LIJUN ZHANG, Doctoral Candidate, and PEISHENG WANG, Master Candidate, are with the State Key Laboratory of Powder Metallurgy, Central South University, Changsha, Hunan, 410083, People's Republic of China. Contact e-mail: yongduyong@gmail.com
Manuscript submitted January 6, 2009.

Article published online July 14, 2009

Table I. Summary of the Experimental Information on the Phase Equilibria in the Alloys Annealed at 600 °C for 40 Days (Atomic Percent)

Number	Nominal Composition			Phases	Composition			Remark
	Mn	Si	Zn		Mn	Si	Zn	
1	26.0	30.0	44.0	Mn ₁₁ Si ₁₉	36.8	63.0	0.2	tie-triangle*
				MnSi	50.0	49.6	0.4	
				liq	4.0	0.4	95.6	
				MnSi	50.1	49.4	0.5	
2	22.5	3.0	74.5	liq	6.5	0.3	93.2	tie-triangle*
				Mn ₅ Si ₃	62.2	37.1	0.7	
				Mn ₅ Si ₃	62.4	36.8	0.8	
				ϵ_2	20.7	0.3	79.0	
3	33.0	0.0	67.0	liq	12.7	0.1	87.2	single phase
				ϵ_1	32.9	0.0	67.1	
4	40.0	10.0	50.0	ϵ_1	34.3	0.2	65.5	tie-line
				Mn ₅ Si ₃	62.4	37.3	0.3	
5	48.0	0.0	52.0	ϵ	47.8	0.0	52.2	single phase
6	65.0	33.0	2.0	Mn ₃ Si	75.1	24.8	0.1	tie-triangle*
				ϵ	41.7	0.2	58.1	
				Mn ₅ Si ₃	62.7	37.1	0.2	
				ν -Mn ₉ Si ₂	80.3	19.1	0.6	
7	75.0	20.0	5.0	Mn ₃ Si	74.8	24.7	0.5	tie-triangle*
				ϵ	47.3	0.1	52.6	
				ν -Mn ₉ Si ₂	81.3	17.9	0.8	
				ϵ	56.2	0.2	43.6	
8	62.0	5.0	33.0	(γ Mn)	66.5	0.0	33.5	tie-line
				ϵ	57.8	0.0	42.2	
9	61.0	0.0	39.0	R-Mn ₆ Si	85.0	13.7	1.3	tie-triangle*
				(γ Mn)	67.3	0.1	32.6	
				ϵ	57.9	0.1	42.0	
11	72.0	0.0	28.0	(γ Mn)	72.3	0.0	27.7	single phase
12	75.0	0.0	25.0	(β Mn)	84.0	0.0	16.0	tie-line
13	73.0	3.0	24.0	(γ Mn)	72.7	0.0	27.3	tie-line*
				R-Mn ₆ Si	87.3	11.7	1.0	
14	79.0	11.0	10.0	(γ Mn)	68.7	0.1	31.2	tie-line*
				R-Mn ₆ Si	84.8	14.1	1.1	
15	87.0	11.0	2.0	ϵ	57.1	0.1	42.8	tie-triangle*
				R-Mn ₆ Si	88.2	11.2	0.6	
				(α Mn)	92.7	6.5	0.8	
				(β Mn)	71.1	0.2	28.7	
16	38.5	0.0	61.5	—	38.6	0.0	61.4	—
17	27.5	0.0	72.5	—	27.7	0.0	72.3	—
18	25.0	0.0	75.0	ϵ_2	25.2	0.0	74.8	single phase
19	23.5	0.0	76.5	ϵ_2	23.8	0.0	76.2	single phase

*Determined by EPMA, and the remaining ones determined by EDX.

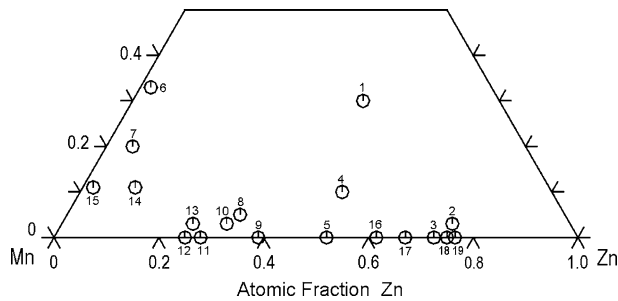


Fig. 1—Nominal compositions of the Mn-Si-Zn alloys.

L4514-type diffusion furnace. After completion of annealing, the alloys were quenched in cold water without breaking quartz tubes but certain alloys selectively by breaking quartz tubes. The metallographic samples were

first examined by using optical microscopy (Leica DMLP, Leica GmbH, Wetzlar, Germany) and scanning electron microscopy with an energy dispersive X-ray spectrometer (SEM/EDX) (JSM-6360LV, JEOL*). Then, some

*JEOL is a trademark of Japan Electron Optics Ltd., Tokyo.

representative alloys were analyzed with an electron probe microanalyzer (JXA-8100, JEOL). The X-ray diffraction (XRD) measurement of the annealed alloys was performed using a Cu K_α radiation on a Rigaku D-max/2550 VB⁺ X-ray diffractometer (Rigaku Corporation, Tokyo, Japan) at 40 kV and 300 mA.

To clarify the controversial phase relations associated with the hcp phase in the Mn-Zn system, two reaction

couples were made with pure Zn and Mn-Zn alloys (as substrate). The two Mn-Zn alloys were alloys 3 (Mn-67 at. pct Zn) and 5 (Mn-52 at. pct Zn), which had already been annealed at 600 °C for 40 days, as previously mentioned. Proper amounts of pure Zn and a piece of Mn-Zn alloy rectangle were put in an alumina crucible that was encapsulated in a quartz tube. The quartz capsules were kept at 600 °C for 2 days in an L4514-type diffusion furnace and subsequently quenched in cold water. The quenched couples were mounted carefully to reveal their exact vertical interfaces. The interfacial reaction products were examined with optical microscopy and SEM /EDX.

III. RESULTS AND DISCUSSION

Table I gives the nominal compositions of the alloys, the phases identified by a combination of XRD and

EDX (or electron microprobe microanalysis (EPMA)), and the phase equilibrium data determined by EPMA and EDX. The backscattered electron images (BEIs) and XRD patterns of the representative ternary alloys, which were annealed at 600 °C for 40 days, are presented in Figures 2 and 3, respectively. The BEI micrographs of two reaction couples are shown in Figure 4.

A. Phase Equilibria of the Boundary Binary Mn-Zn System at 600 °C

To investigate the phase equilibria of the boundary binary Mn-Zn system at 600 °C, nine equilibrated Mn-Zn alloys were made, and two of them were used to prepare reaction couples with pure Zn.

As listed in Table I, the tie-line data of the two-phase equilibrium between (γ Mn) and ϵ were determined with

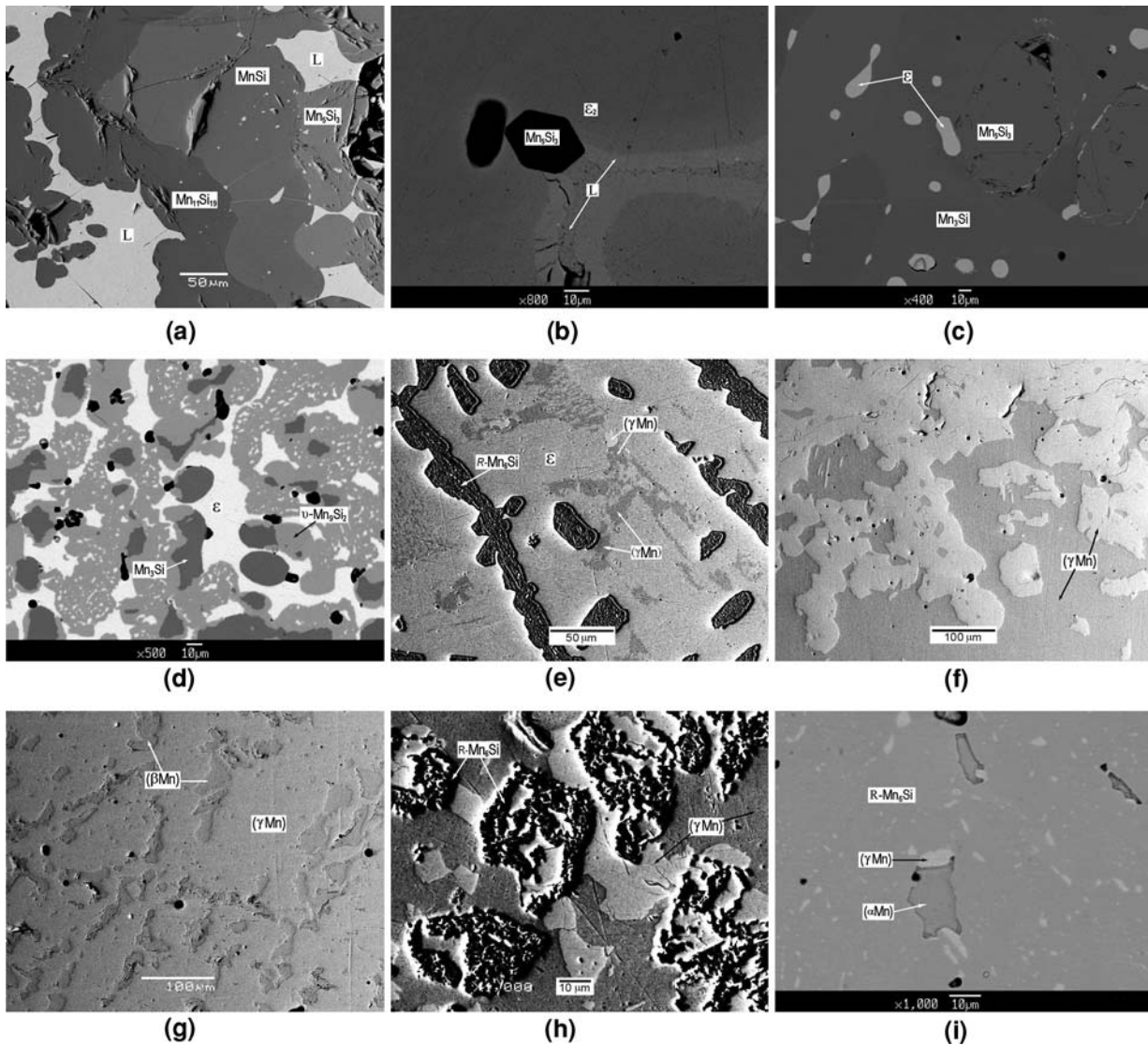


Fig. 2—Microstructures of the representative alloys annealed at 600 °C for 40 days: (a) alloy 1 ($\text{Mn}_{26.0}\text{Si}_{30.0}\text{Zn}_{44.0}$), magnification 300 times; (b) alloy 2 ($\text{Mn}_{22.5}\text{Si}_{33.0}\text{Zn}_{74.5}$), magnification 800 times; (c) alloy 6 ($\text{Mn}_{65.0}\text{Si}_{33.0}\text{Zn}_{2.0}$), magnification 400 times; (d) alloy 7 ($\text{Mn}_{75.0}\text{Si}_{20.0}\text{Zn}_{5.0}$), magnification 500 times; (e) alloy 10 ($\text{Mn}_{65.5}\text{Si}_{33.0}\text{Zn}_{31.5}$), magnification 400 times; (f) alloy 11 ($\text{Mn}_{72.0}\text{Zn}_{28.0}$), magnification 200 times; (g) alloy 12 ($\text{Mn}_{75.0}\text{Zn}_{25.0}$), magnification 230 times; (h) alloy 13 ($\text{Mn}_{73.0}\text{Si}_{3.0}\text{Zn}_{24.0}$), magnification 1000 times; (i) alloy 15 ($\text{Mn}_{87.0}\text{Si}_{11.0}\text{Zn}_{2.0}$), magnification 1000 times.

alloy 9 ($\text{Mn}_{61.0}\text{Zn}_{39.0}$). Figure 2(f) is the BEI micrograph of alloy 11 ($\text{Mn}_{72.0}\text{Zn}_{28.0}$), which was quenched in cold water without breaking quartz tubes. Two different phase regions, which had obvious color contrast and hardness difference as well as slight composition difference, were observed in alloy 11, as shown in Figure 2(f), even though this alloy is located in the single-phase area of (γ Mn). Figure 2(g) is the BEI micrograph of alloy 12 ($\text{Mn}_{75.0}\text{Zn}_{25.0}$), which was quenched in cold water by breaking quartz tubes so as to raise the cooling rate. Two different phase regions corresponding to (β Mn) and (γ Mn) were observed in alloy 12. The phase equilibrium compositions for (β Mn) and (γ Mn) were determined to be Mn-16.0 at. pct Zn and Mn-27.3 at. pct Zn, respectively. It should be noted, however, that with the cooling rate elevated, the aforementioned phenomenon in alloy 11 was no more observed in alloy 12. Therefore, the case for alloy 11 could be ascribed to massive phase transformation arising from its slow quenching. Compared to Okamoto,^[3] the presently determined two-phase field for (β Mn) and (γ Mn) is considerably larger than the former.

Six Mn-Zn binary alloys (*viz.* alloys 3, 5, and 16 through 19) given in Table I were designed to investigate the controversial hexagonal ϵ phase. In addition, results on seven Mn-Si-Zn ternary alloys (*viz.* alloys 2, 4, 6 through 8, 10, and 14) related to the ϵ phase could throw light on the ϵ phase too. The phase separation of the ϵ phase reported by Wachtel and Tsiuplakis^[6] was not observed in these alloys *via* XRD identification and SEM microstructural examination. According to

Okamoto and Tanner,^[5] alloys 16 ($\text{Mn}_{38.5}\text{Zn}_{61.5}$) and 17 ($\text{Mn}_{27.5}\text{Zn}_{72.5}$) are in the two-phase regions of $\epsilon + \epsilon_1$ and $\epsilon_1 + \epsilon_2$, respectively. However, upon SEM/EDX examination, the ϵ_1 and ϵ_2 phases separated from the ϵ phase were not observed in these two alloys. Alloy 19 ($\text{Mn}_{23.5}\text{Zn}_{76.5}$) is in the single-phase region of ϵ_2 , according to Okamoto and Tanner.^[5] The XRD pattern of alloy 19, which is very close to that of alloy 18 ($\text{Mn}_{25.0}\text{Zn}_{75.0}$), is shown in Figure 3(a) together with that of alloy 4 ($\text{Mn}_{40.0}\text{Si}_{10.0}\text{Zn}_{50.0}$), which is located in the two-phase region of $\text{Mn}_5\text{Si}_3 + \epsilon_1$, according to Okamoto and Tanner.^[5] As shown in Figure 3(a), only the ϵ phase with a PDF number 65-7463 was indexed both in alloy 19 and in alloy 4. It should be noted, nevertheless, that alloys 18 and 19, which can be easily ground, were much more brittle than four additional Mn-Zn alloys (*viz.* alloys 3, 5, and 16 and 17). It was reported that three divisions for ϵ , ϵ_1 , and ϵ_2 were established by Reumont *et al.*^[8] on the 450 °C Fe-Mn-Zn isothermal section, which is in accord with Wachtel and Tsiuplakis.^[6] However, convincing evidence was not presented to support their conclusion.

Figures 4(a) and (b) are the BEI micrographs of the two reaction couples of alloy 3 with pure Zn and of alloy 5 with pure Zn, respectively. The experimental results showed that both alloy 3 ($\text{Mn}_{33.0}\text{Zn}_{67.0}$) and alloy 5 ($\text{Mn}_{48.0}\text{Zn}_{52.0}$) are in single-phase regions, which is in accordance with the evaluated phase diagram by Okamoto and Tanner.^[5] No newly formed intermetallic phase was observed in the interdiffusion zone of the former couple. However, a newly formed intermetallic phase

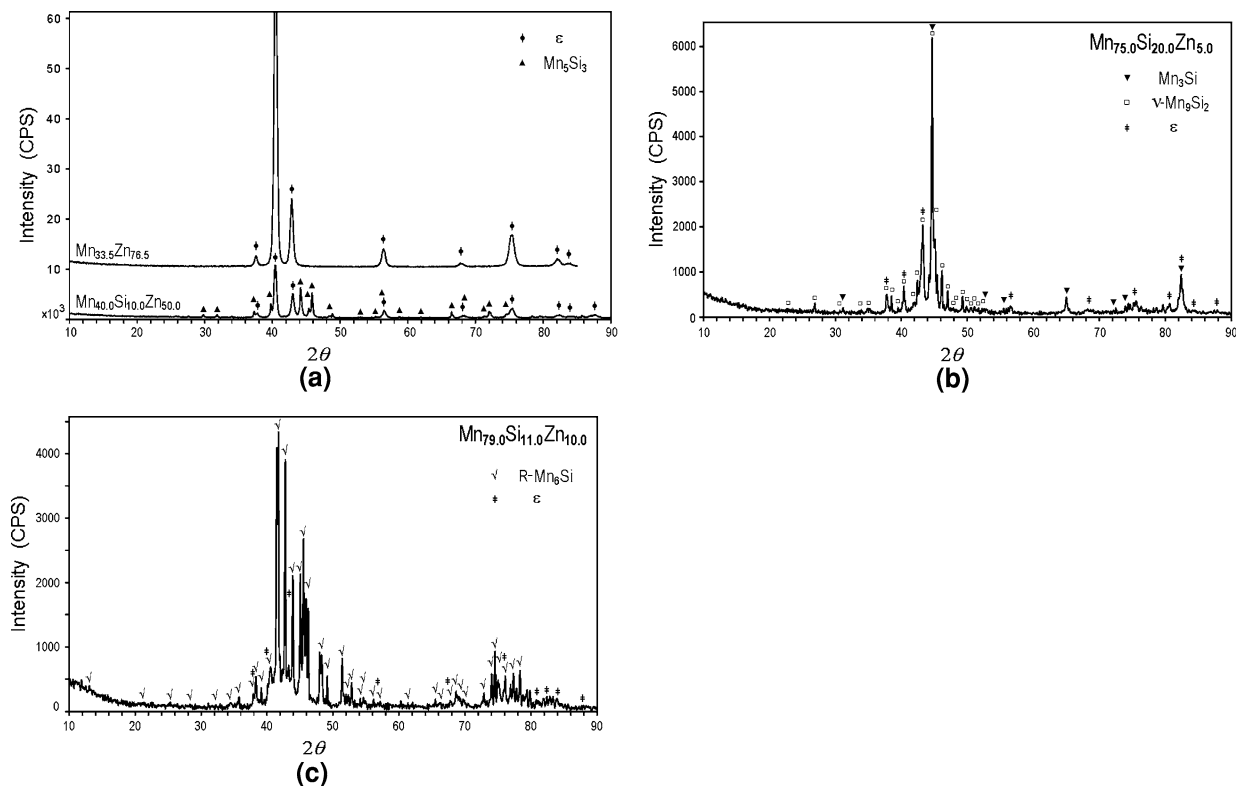
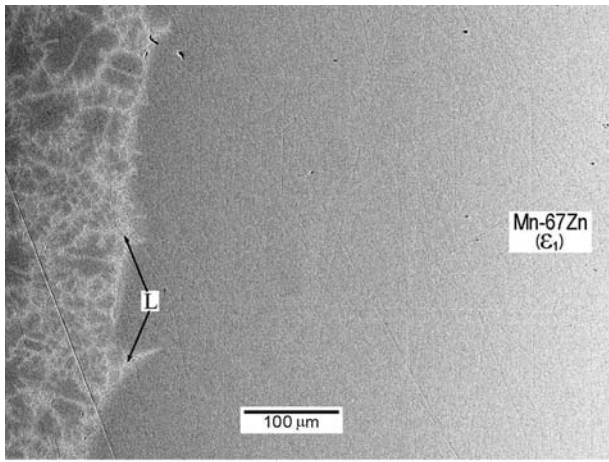
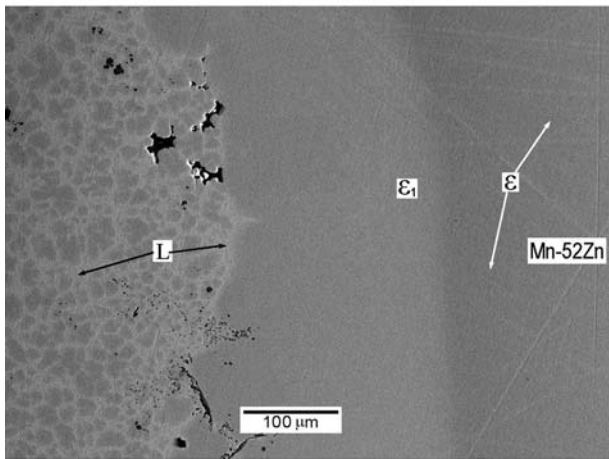


Fig. 3—XRD patterns of the representative alloys annealed at 600 °C for 40 days: (a) alloys 4 ($\text{Mn}_{40.0}\text{Si}_{10.0}\text{Zn}_{50.0}$) and 19 ($\text{Mn}_{23.5}\text{Zn}_{76.5}$), (b) alloy 7 ($\text{Mn}_{75.0}\text{Si}_{20.0}\text{Zn}_{5.0}$), and (c) alloy 14 ($\text{Mn}_{79.0}\text{Si}_{11.0}\text{Zn}_{10.0}$).



(a)



(b)

Fig. 4—Microstructures of two reaction diffusion couples annealed at 600 °C for 2 days: (a) Zn/(Mn-67Zn), magnification 200 times; and (b) Zn/(Mn-52 Zn), magnification 200 times.

corresponding to ϵ_1 in Reference 5 was observed in the latter couple, as a concentration jump occurred at the interface of ϵ and ϵ_1 , as shown in Figure 4(b). Since the phase boundaries for ϵ and ϵ_1 were not accurately measured in the present work, the corresponding two-phase field for the ϵ and ϵ_1 is shown in Figure 5 with dashed lines. In addition, the ϵ_2 division of the ϵ phase, which was proposed by Wachtel and Tsiuplakis,^[6] is assumed to exist and is shown in Figure 5 with dashed lines, taking into account the difference in the observed mechanical properties of the Mn-Zn binary alloys.

B. Isothermal Section of the Mn-Si-Zn System at 600 °C

Figure 5 is the isothermal section at 600 °C of the Mn-Si-Zn system, which is constructed based on the present results and the information available from the phase diagrams of the boundary binary systems.^[2,3,5]

The experimental results showed no existence of ternary compounds in the Mn-Si-Zn system. The following eight three-phase fields were well determined:

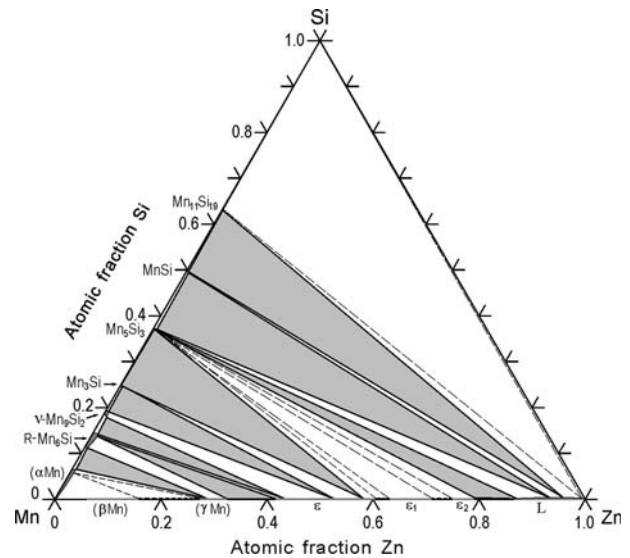


Fig. 5—Isothermal section at 600 °C of the Mn-Si-Zn system.

(1) $\text{Mn}_{11}\text{Si}_{19} + \text{MnSi} + \text{L}$, (2) $\text{MnSi} + \text{Mn}_5\text{Si}_3 + \text{L}$, (3) $\text{Mn}_5\text{Si}_3 + \text{L} + \epsilon_2$, (4) $\text{Mn}_5\text{Si}_3 + \epsilon + \text{Mn}_3\text{Si}$, (5) $\text{Mn}_3\text{Si} + \epsilon + \nu\text{-Mn}_9\text{Si}_2$, (6) $\nu\text{-Mn}_9\text{Si}_2 + \epsilon + \text{R-Mn}_6\text{Si}$, (7) $\epsilon + \text{R-Mn}_6\text{Si} + (\gamma\text{Mn})$, and (8) $\text{R-Mn}_6\text{Si} + (\alpha\text{Mn}) + (\gamma\text{Mn})$. Three subdivisions of the hexagonal ϵ phase (*viz.* ϵ , ϵ_1 , and ϵ_2), reported by Wachtel and Tsiuplakis,^[6] are accepted and the three-phase equilibria for $\text{Mn}_5\text{Si}_3 + \epsilon + \epsilon_1$ and $\text{Mn}_5\text{Si}_3 + \epsilon_1 + \epsilon_2$ shown in Figure 5 with dashed lines indicating their uncertainty. The remaining three-phase fields, which were not well determined or deduced, are also shown with dashed lines in Figure 5.

As shown in Figure 2(a), there occurred four phases in alloy 1 ($\text{Mn}_{26.0}\text{Si}_{30.0}\text{Zn}_{44.0}$), from which two sets of the experimental data of the three-phase equilibria ($\text{MnSi} + \text{Mn}_5\text{Si}_3 + \text{L}$ and $\text{Mn}_{11}\text{Si}_{19} + \text{MnSi} + \text{L}$) were determined. The white Zn-rich area in Figure 2(a), which was in liquid state at 600 °C, is still marked as “L,” although it was solidified during quenching.

Figure 2(b) is the BEI micrograph of alloy ($\text{Mn}_{22.5}\text{Si}_{3.0}\text{Zn}_{74.5}$), which was characterized as three phases, *viz.* Mn_5Si_3 , ϵ_1 , and liquid. The microstructures and EPMA results of alloy 6 ($\text{Mn}_{65.0}\text{Si}_{33.0}\text{Zn}_{2.0}$), which are shown in Figure 2(c) and listed in Table I, respectively, revealed that alloy 6 is located in the three-phase equilibrium region of $\text{Mn}_5\text{Si}_3 + \epsilon + \text{Mn}_3\text{Si}$. In other words, the Mn_5Si_2 phase was not observed at 600 °C.

The microstructures (Figure 2(d)), XRD pattern (in Figure 3(b)), and EPMA results (Table I) of alloy 7 ($\text{Mn}_{75.0}\text{Si}_{20.0}\text{Zn}_{5.0}$) showed that Mn_3Si , ϵ , and $\nu\text{-Mn}_9\text{Si}_2$ are in three-phase equilibrium. The experimental results of alloy 10 ($\text{Mn}_{65.5}\text{Si}_{33.0}\text{Zn}_{31.5}$) suggested that $\text{R-Mn}_6\text{Si}$, (γMn) and ϵ are in three-phase equilibrium, as shown in Figure 2(e). Based on the XRD results of alloy 14 ($\text{Mn}_{79.0}\text{Si}_{11.0}\text{Zn}_{10.0}$) shown in Figure 3(c) and the results of alloy 8 ($\text{Mn}_{62.0}\text{Si}_{5.0}\text{Zn}_{33.0}$) listed in Table I, it can be deduced that $\nu\text{-Mn}_9\text{Si}_2$, ϵ , and $\text{R-Mn}_6\text{Si}$ are in three-phase equilibrium.

It should be mentioned that massive phase transformation, which was observed in alloy 11 ($\text{Mn}_{72.0}\text{Zn}_{28.0}$),

as previously stated, was also observed in alloys 10 ($\text{Mn}_{65.5}\text{Si}_{3.0}\text{Zn}_{31.5}$) and 13 ($\text{Mn}_{73.0}\text{Si}_{3.0}\text{Zn}_{24.0}$) quenched in cold water without breaking quartz tubes. Figure 2(h) is the BEI micrograph of alloy 13, in which the compositions of the gray phase and light gray phase were measured to be almost the same. Though this case was also observed in alloy 10, as seen in Figure 2(e), the quantity of the light gray phase was overwhelmingly smaller than that of the dark gray phase. Figure 3(i) is the BEI micrograph of alloy 15 ($\text{Mn}_{87.0}\text{Si}_{11.0}\text{Zn}_{2.0}$). The experimental results indicated that R-Mn₆Si, (α Mn) and (γ Mn) are in three-phase equilibrium.

IV. CONCLUSIONS

The isothermal section at 600 °C of the Mn-Si-Zn system was determined *via* nineteen equilibrated alloys and two diffusion couples.

The experimental results showed no existence of ternary compounds in the Mn-Si-Zn system. Mn₅Si₂ was not observed at 600 °C. A massive phase transformation for (γ Mn) was observed due to its slow quenching. The existence of ε_1 , which is controversial in the literature, was confirmed through a diffusion couple method. Although the existence of ε_2 (another controversial division of the ε phase) was not confirmed, it is assumed to exist, taking into account the difference in the observed mechanical properties of the Mn-Zn binary alloys.

The following eight three-phase equilibria were well determined: (1) Mn₁₁Si₁₉ + MnSi + L, (2) MnSi + Mn₅Si₃ + L, (3) Mn₅Si₃ + L + ε_2 , (4) Mn₅Si₃ + ε +

Mn₃Si, (5) Mn₃Si + ε + ν -Mn₉Si₂, (6) ν -Mn₉Si₂ + ε + R-Mn₆Si, (7) ε + R-Mn₆Si + (γ Mn), and (8) R-Mn₆Si + (α Mn) + (γ Mn). The solubility of Zn in R-Mn₆Si, ν -Mn₉Si₂, Mn₃Si, Mn₅Si₃, MnSi, and Mn₁₁Si₁₉ were measured to be 1.3, 0.8, 0.5, 0.8, 0.5, and 0.2 at pct Zn, respectively. The solubility of Si in (β Mn), (γ Mn), ε , and liquid were determined to be negligible.

ACKNOWLEDGMENTS

The financial support from the National Basic Research Program of China (Grant No. 2006CB6 00906) and the Creative Research Group of National Natural Science Foundation of China (Grant No. 50721003) is acknowledged.

REFERENCES

1. E.D. Bruycker, B.C. De Cooman, and M.D. Meyer: *Steel Res. Int.*, 2004, vol. 5, pp. 147–52.
2. M.H.G. Jacobs and P.J. Spencer: *CALPHAD*, 1996, vol. 20, pp. 307–20.
3. H. Okamoto: *J. Phase Equilib.*, 1991, vol. 12, pp. 505–07.
4. Y. Du, J.C. Schuster, F. Weitzer, N. Krendelsberger, B.Y. Huang, Z.P. Jin, W.P. Gong, Z.H. Yuan, and H.H. Xu: *Metall. Mater. Trans. A*, 2004, vol. 35A, pp. 1613–28.
5. H. Okamoto and L.E. Tanner: *Bull. Alloy Phase Diagrams*, 1990, vol. 11, pp. 377–84.
6. E. Wachtel and K. Tsiuplakis: *Z. Metallkd.*, 1967, vol. 58, pp. 41–45.
7. O. Romer and E. Wachtel: *Z. Metallkd.*, 1971, vol. 62, pp. 820–25.
8. Y. Nakagawa and T. Hori: *Trans. Jpn. Inst. Met.*, 1972, vol. 13, pp. 167–70.
9. G. Reumont, G. Dupont, and P. Perrot: *Z. Metallkd.*, 1995, vol. 86, pp. 608–13.